

Oct 27, 2020

Dear Editor,

According to you and the reviewer's suggestion for technical corrections of our manuscript, we added some text to explain the model domain settings *in Section Model configuration and experiments*, and also discussed the model domain might be small while explaining the impact of atmospheric circulation related to the Tibetan Plateau on air quality *in Conclusions*. The details refer to the following response.

Thank you very much for handling our paper.

Best regards,

Xuexi Tie

Reply to Anonymous Referee

Thanks for the reviewer's helpful suggestions. We have given technical corrections to the size of the model domain in the revised manuscript.

Technical Corrections

The authors conclude that the warming TP or cooling TP will have similar effects on air quality in Sichuan Basin. However, I think that the simulation domain may be too small to reveal the effect of TP on air quality in Sichuan Basin. The Sichuan Basin is located nearby the boundary of the simulation domain. It is better to simulate the experiments at a wider range and make the Sichuan Basin and TP located in the center of domain. In this way, we can comprehensively see changes in atmospheric circulation over the TP and its effects on local circulation in Sichuan Basin.

Corrections: We have added the text to explain the model domain settings in Lines 140-146: *“Ideally, this study should set the Tibetan Plateau and the Sichuan Basin as the center of the model domain. However, considering the domain is too large, beyond the capability of our computer, we have to reduce the model domain. Nonetheless, to better simulate the atmospheric circulation over the plateau and its impact on air quality in the Sichuan Basin, we set the central location of the model domain at 95.0°E, 32.2°N over the plateau, and the simulation domain covers the Tibetan Plateau and the Sichuan Basin (Figure 1).”*

We also discussed the limitation of the model domain in Lines 476-484: *“Here we need to clarify that our model domain may be a little small to comprehensively atmospheric circulation pattern related to the Tibetan Plateau and the subsequent impact on air quality in the Sichuan Basin, though the domain covers the plateau and the basin. We notice that the basin is nearby the eastern boundary of the domain, in which local circulation might be influenced by the lateral condition. Therefore, as the plateau is likely to continue*

warming, in-depth understanding to climate change on the Tibetan Plateau and long-term PM_{2.5} measurements are required to validate the impact of the warming plateau on air quality in a larger spatial scale.”

1 **The Warming Tibetan Plateau improves winter air quality in the Sichuan Basin,**
2 **China**

3

4 Shuyu Zhao¹, Tian Feng², Xuexi Tie^{1,3*}, Zebin Wang⁴

5

6 ¹Key Laboratory of Aerosol Chemistry and Physics, SKLLQG, Institute of Earth
7 Environment, Chinese Academy of Sciences, Xi'an, 710061, China

8 ²Department of Geography & Spatial Information Techniques, Ningbo University,
9 Ningbo, 315211, China

10 ³Center for Excellence in Urban Atmospheric Environment, Institute of Urban
11 Environment, Chinese Academy of Sciences, Xiamen, 361021, China

12 ⁴Northwest Air Traffic Management Bureau, Civil Aviation Administration of China,
13 Xi'an, 712000, China

14

15 Corresponding author: tiexx@ieecas.cn

16

17 **Key points**

18

19 The Tibetan Plateau is rapidly warming, and the temperature has risen by 2 ° C from
20 2013 to 2017.

21

22 A warming plateau leads to an enhanced easterly wind, an increased PBLH and a
23 decreased RH in the Sichuan Basin.

24

25 The 2 ° C warming significantly reduces PM_{2.5} concentration in the basin by 25.1 µg
26 m⁻³, of which secondary aerosol is 19.7 µg m⁻³.

27

28 **Abstract**

29

30 Impacts of global climate change on the occurrence and development of air pollution
31 have attracted more attentions. This study investigates impacts of the warming Tibetan
32 Plateau on air quality in the Sichuan Basin. Meteorological observations and ERA-
33 interim reanalysis data reveal that the plateau has been rapidly warming during the last
34 40 years (1979-2017), particularly in winter when the warming rate is approximately
35 twice as much as the annual warming rate. Since 2013, the winter temperature over the
36 plateau has even risen by 2 ° C. Here we use the WRF-CHEM model to lay emphasis
37 on the impact of the 2 ° C warming on air quality in the basin. The model results show
38 that the 2 ° C warming causes an enhanced easterly wind, an increase in the Planetary
39 Boundary Layer height (PBLH) and a decrease in the relative humidity (RH) in the
40 basin. Enhanced easterly wind increases PM_{2.5} transport from the basin to the plateau.
41 The elevated PBLH strengthens vertical diffusion of PM_{2.5}, while the decreased RH
42 significantly reduces secondary aerosol formation. Overall, PM_{2.5} concentration is
43 reduced by 17.5% (~25.1 μg m⁻³), of which the reduction in primary and secondary
44 aerosols is 5.4 μg m⁻³ and 19.7 μg m⁻³, respectively. These results reveal that the recent
45 warming plateau has improved air quality in the basin, to some certain extent,
46 mitigating the air pollution therein. Nevertheless, climate system is particularly
47 complicated, and more studies are needed to demonstrate the impact of climate change
48 on air quality in the downstream regions as the plateau is likely to continue warming.

49

50 **Keywords:** climate change, air quality, Tibetan Plateau, WRF-CHEM model

51

52 **1 Introduction**

53

54 The Tibetan Plateau is known as the third pole because of its high altitude and large
55 area. It is also regarded as an important response region to the Northern Hemisphere,
56 and even global climate due to its sensitivity to climate change. Previous studies on the
57 Tibetan Plateau show that the region was experiencing warming in the second half of
58 the 20th century, especially in the winter months (Kuang and Jiao, 2016; Liu and Chen,
59 2000; Rangwala et al., 2009). The warming plateau not only plays a significant role in
60 driving the weather and climate change, as well as the ecological system, but also has
61 an important impact on air quality in the downstream regions. Xu et al. (2016) suggest
62 that the thermal anomaly over the Tibetan Plateau obviously increases haze frequency
63 and surface aerosol concentration in central-eastern China.

64

65 However, the impacts of climate change on air quality in China are still unclear. Some
66 researches hold the opinion that climate change induced by greenhouse gas emission
67 increases severe haze occurrence and intensity in winter at Beijing, and its impact will
68 continue in the future (Cai et al., 2017; Zou et al., 2017). Similarly, Xu et al. (2017)
69 suggest that climate warming anomaly in the lower and middle troposphere over the
70 continent around the Yangtze River Delta leads to more haze days in winter during
71 recent decades. On the contrary, another opinion suggests that climate change in the
72 past two decades is favorable for air pollution dispersion in northern China via
73 enhancing mid-latitude cold surges in winter (Zhao et al., 2018). If cold surge is strong
74 enough, pollutants would be transported to the downstream regions, causing a better air
75 quality in the upstream region but a worse one in the downstream region. Thus, there
76 may be regional differences in the impact of climate change on air quality.

77

78 Previous studies on air pollution in China are concentrated in the developed regions,

79 such as the North China Plain, the Yangtze River Delta and the Pearl River Delta. Few
80 studies have paid attention to the Sichuan Basin, although the region is undergoing
81 severe air pollution, and mean PM_{2.5} concentration is more than 110 µg m⁻³ in winter
82 (Qiao et al., 2019; Tao et al., 2017; Wang et al., 2018; Yang et al., 2011). Thus, it is
83 necessary to explore the underlying causes that leads to air pollution in the Sichuan
84 Basin.

85

86 The Sichuan Basin locates in the downstream region of the Tibetan Plateau, and its
87 weather conditions are obviously affected by the plateau (Duan et al., 2012; Hua, 2017;
88 Zhao et al., 2019). For instance, the foggy weather, southwest vortex and low-level
89 shear line over the basin are closely associated with the plateau (Zhu et al., 2000). These
90 changes in weather conditions induced by the plateau undoubtedly affect the
91 development and dispersion of air pollution in the basin, because the huge terrain can
92 trigger a thermodynamic forcing, which is of great importance for weather conditions
93 in the surrounding regions (Bei et al., 2016; 2017; Zhao et al., 2015).

94

95 This study therefore focuses on how climate change on the Tibetan Plateau affects air
96 quality in the Sichuan Basin in recent years. Section 3 analyzes the temperature change
97 on the plateau in the past four decades, and especially emphasizes the change in recent
98 five years. In Section 4, we design three sets of numerical simulations to calculate the
99 impact of temperature change on air quality. One group includes two baseline
100 simulations in two periods (January 2014 and January 2018), which are constrained by
101 observed surface meteorological parameters and pollutant concentrations. The second
102 group includes three sensitivity simulations during the 2013-2014 winter, which uses
103 the same emission inventory and meteorological fields as the baseline simulation in
104 January 2014 except for a changed air temperature. We also set the third sensitivity
105 simulation, in which the plateau is also warming, but on the basis of the period for the
106 2017-2018 winter. We compare the difference in PM_{2.5} concentrations in these cases,

107 and also calculate differences in meteorological parameters that include winds (wind
108 speed and direction), air temperature, and relative humidity (RH), as well as the
109 Planetary Boundary Layer height (PBLH). Based on the differences in PM_{2.5}
110 concentration and meteorological parameters above, we finally explain the cause-to-
111 effect relationship between a warming plateau and changes in the winds, PBLH and RH
112 in the Sichuan Basin. Moreover, we calculate the effect of the relationship on air quality
113 in the basin.

114

115 **2 Data and Methods**

116

117 **2.1 Observations**

118

119 To ensure a robust result, we use two datasets of surface air temperature in this study.
120 One is the European Center for Medium-Range Weather Forecasts (ECMWF) ERA-
121 Interim monthly mean reanalysis data (1979-2018), obtained from the website of
122 <http://apps.ecmwf.int/datasets/>, with the finest horizontal resolution of 0.125°×0.125°.
123 The other is hourly and monthly mean weather-station observations from the National
124 Oceanic and Atmospheric Administration (NOAA), available from
125 <http://gis.ncdc.noaa.gov/map/viewer/#app=clim&cfg=cdo&theme=hourly&layers=1>
126 <http://gis.ncdc.noaa.gov/map/viewer/#app=clim&cfg=cdo&theme=hourly&layers=1>
&node=gis.

127

128 Figure 1 shows the distribution of weather stations over the Tibetan Plateau, and these
129 weather stations widely cover the entire plateau. Trends of annual mean and winter
130 surface air temperature over the plateau are analyzed, and the winter is averaged over
131 3-month periods (December-January-February). Additionally, we use ambient air
132 quality data to validate the model performance. Since 2013, the data are released by
133 Ministry of Environmental Protection, China at <http://www.aqistudy.cn/>, including
134 hourly PM_{2.5}, CO, and O₃ mass concentrations. The monitoring stations for air quality

135 are also shown in Figure 1.

136

137 **2.2 Model configuration and experiments**

138

139 A state-of-the-art regional dynamical and chemical model (WRF-CHEM model) is used
140 in the study. Ideally, this study should set the Tibetan Plateau and the Sichuan Basin as
141 the center of the model domain. However, considering the domain is too large, beyond
142 the capability of our computer, we have to reduce the model domain. Nonetheless, to
143 better simulate the atmospheric circulation over the plateau and its impact on air quality
144 in the Sichuan Basin, we set the central location of the model domain at 95.0°E, 32.2°N
145 over the plateau, and the simulation domain covers the Tibetan Plateau and the Sichuan
146 Basin (Figure 1). The Tibetan Plateau covers about 2.5 million km², with the averaged
147 elevation of 4500 m, and the Sichuan Basin covers about 0.16 million km², with the
148 elevation in the center of the basin less than 1000 m (250 - 700 m). The model is set by
149 a horizontal grid resolution of 9 km (451 × 221 grids), with 35 vertical sigma levels.
150 The model description in detail is seen by Grell et al. (2005). The evaluation of the
151 model performance has been conducted by many previous studies (Li et al., 2011a; Tie
152 et al., 2009; 2007). In this study, we use the Goddard longwave and shortwave radiation
153 parameterization (Dudhia, 1989), the WSM 6-class graupel microphysics scheme
154 (Hong and Lim, 2006), the Mellor-Yamada-Janji (MYJ) planetary boundary layer
155 scheme (Janjić, 2002), the unified Noah land-surface model (Chen and Dudhia, 2001)
156 and Monin-Obukhov surface layer scheme (Janjić, 2002). For chemical schemes, we
157 use a new flexible gas-phase chemical module and the Community Multiscale Air
158 Quality (CMAQ, version 4.6) aerosol module developed by the US EPA (Binkowski,
159 2003). Gas-phase atmospheric reactions of volatile organic compounds (VOCs) and
160 nitrogen oxide (NO_x) use the SAPRC-99 (Statewide Air Pollution Research Center,
161 version 1999) chemical mechanism. Inorganic aerosols use the ISORROPIA version
162 1.7, referring to Li et al. (2011a) and Feng et al. (2016). A SO₂ heterogeneous reaction

163 mechanism on aerosol surfaces involving aerosol water is added (Li et al., 2017a), and
164 NO₂ heterogeneous reaction to produce HONO is also considered (Li et al., 2010). The
165 secondary organic aerosol (SOA) calculation uses a non-traditional volatility basis-set
166 approach by Li et al. (2011b). The photolysis rates are calculated by a fast Tropospheric
167 Ultraviolet and Visible (FTUV) radiation transfer model, in which the impacts of
168 aerosols and clouds on the photochemistry processes are considered (Li et al., 2011a;
169 Tie et al., 2003; 2005). The wet deposition is calculated by the method used in CMAQ
170 and the dry deposition follows Wesely (1989).

171

172 We use the MIX anthropogenic emission inventory for the year of 2010, and it is
173 available at Multi-resolution Emission Inventory for China
174 (<http://www.meicmodel.org/dataset-mix.html>), consisting of industrial, power,
175 transportation, and agricultural as well as residential sources (Li et al., 2017b; Zhang
176 et al., 2009). The emission inventory is constructed by a ‘bottom-up’ approach based
177 on national and provincial activity data and emission factors. To improve the emission
178 inventory accuracy, we use a ‘top-down’ method here to constrain the emission
179 inventory. We compare the simulated value with the measured value time and again
180 until the simulations are close to the measurements. The biogenic emissions are online
181 calculated by the Model of Emissions of Gases and Aerosol from Nature (MEGAN)
182 (Guenther et al., 2006). Initial and boundary meteorological fields in the model are
183 driven by 6-hour 1° × 1° NCEP (National Centers for Environmental Prediction)
184 reanalysis data. Chemical lateral conditions are provided by a global chemistry
185 transport model – MOZART (Model for OZone And Related chemical Tracer, version
186 4), with a 6-h output (Emmons et al., 2010; Tie et al., 2005). The spin-up time of the
187 WRF-CHEM model is 1 day.

188

189 According to the meteorological records at weather stations, surface air temperature
190 risen by an average of 2°C from 2013 to 2017 over the plateau (Table S1). ERA-

191 interim reanalysis data also show that the troposphere (600hPa - 250hPa) over the
192 plateau is warming during the 2013-2017 period, and the temperature increment shows
193 a parabolic pattern with the altitude, by an average increase of $\sim 2^{\circ}\text{C}$ (Figure S1). Thus,
194 we design several sensitivity simulations, with an average temperature increase in the
195 troposphere over the plateau, to assess impacts of a warming plateau on air quality in
196 the basin. To eliminate the influence of simulation background, we conduct two
197 baseline simulations for the 2013-2014 winter (January 2014) and the 2017-2018
198 winter (January 2018) as the control groups. The other two sets focus on sensitivity
199 simulations that reflect an observational increase in air temperature over the plateau.
200 At the year of 2014, the sensitivity simulation uses the same emission inventory and
201 meteorological conditions as the baseline simulation except that the temperature in the
202 troposphere over the plateau respectively increases by 0.5°C , 1.0°C and 2.0°C . The
203 third group is a sensitivity simulation with an increase of 2.0°C on the basis of air
204 temperature in January 2018. In the domain, we set to the warming at all grids covering
205 the plateau (the region surrounded by the dark line in Figure 1b) in the initial and
206 boundary fields. In order to ensure a persistent influence of the warming, we drive the
207 initial field with a 0.5°C , 1.0°C , and 2°C increment every day in January 2014, and a
208 2°C increment every day in January 2018. Then, by comparing the difference between
209 the sensitivity simulations and the baseline simulation, we determine the impact of the
210 warming over the plateau on air quality in the basin.

211

212 **3 The warming Tibetan Plateau in the last four decades**

213

214 Figure 2 shows the variability and linear trend of surface air temperature at 10 weather
215 stations over the Tibetan Plateau in winter during the last four decades (1979 - 2017).
216 The winter mean temperature recorded from all the weather stations exhibits an
217 obvious annual fluctuation and the linear regression shows a significant rising trend.
218 Clearly, the plateau is continuously undergoing a warming phase, albeit with regional

219 differences in the warming magnitude. The warming rates in different regions vary in
220 the range of 0.5 - 1.0°C decade⁻¹. Compared with the warming rate of annual mean
221 temperature (Figure S2), the warming rate in winter is approximately twice as much,
222 suggesting that the warming in winter is more significant.

223

224 Using the ERA-interim reanalysis data, Figure 3 shows the temperature change during
225 the same period (1979 - 2017). The result is consistent with weather records, showing
226 that air temperature is significantly rising in most parts of the plateau. The maximal
227 warming rate is around 0.6 - 0.8°C decade⁻¹, appeared in the central and southern
228 plateau. The warming in the rest areas is slighter, with a rate of 0.3 - 0.6 °C decade⁻¹.
229 Particularly, the averaged warming rate in the vast central plateau reaches about 1.0°C
230 yr⁻¹ in recent five years (Figure S3), greater than the warming rate during the entire 40
231 years (Figure 3). Both the observation records and reanalysis data evidently show that
232 the plateau has been warming in the last four decades, and also the warming trend for
233 recent years is more significant.

234

235 From the above temperature change analysis, we notice that there is obviously a
236 positive temperature anomaly between 2013 and 2017 winters, implying for an
237 accelerating warming over the plateau. The observational temperature in winter
238 increases by about 2°C between 2013 and 2017. Therefore, we assess the impact of a
239 warming plateau on air quality in the Sichuan Basin.

240

241 **4 Results and Discussion**

242

243 **4.1 Model validation**

244

245 To systemically evaluate the model performance on simulation O₃, CO and PM_{2.5} mass
246 concentrations, three statistical indices are used. They are the mean bias (MB), root

247 mean square error (RMSE), and index of agreement (IOA). The calculation formulas
248 are given in Text S1. The IOAs of air temperature and RH are 0.85 and 0.79,
249 respectively (Figure S4a and Figure S4b), suggesting that the model well captures the
250 diurnal cycle of temperature and the variability of RH. However, the calculated wind
251 speed is overestimated, especially in the region between the Tibetan Plateau and the
252 Sichuan Basin. This is because there is a dramatic elevation drop in the region, which
253 makes it difficult for the model to replicate the observed wind speed and direction.

254

255 Figure 4 shows comparisons of hourly O₃, CO and PM_{2.5} concentrations between the
256 model simulations and measurements. The result shows that the simulated CO mean
257 level is close to the measurement, with a MB of 0.11 mg m⁻³, indicating that the model
258 reasonably reproduces the meteorological fields and long-range transport. Because the
259 chemical lifetime of CO is relatively long (~months), the variability of CO is
260 dominantly determined by the meteorological fields and atmospheric transport process.
261 For the simulation of O₃, in addition to the effects of meteorological fields and
262 atmospheric transport process, its variability is strongly controlled by the
263 photochemical process. The model result shows that the simulated diurnal cycle of O₃
264 is reasonably agreed with the measurement, with an IOA of 0.79. There is only a small
265 bias between the simulated and measured O₃ mean concentration. The simulated O₃
266 concentration is 1.7 μg m⁻³ higher than the measurement, suggesting that both the
267 photochemistry and long-range transport well capture the O₃ variability in the region.
268 Finally, the IOA between the simulated and measured PM_{2.5} concentrations is 0.80,
269 indicating that the aerosol module in the model generally captures the measured PM_{2.5}
270 variation.

271

272 However, there are some noticeable discrepancies between the simulations and the
273 measurements. For instance, the simulated magnitude of PM_{2.5} concentration is larger
274 than the measurement, and its mean level is underestimated by 13.1 μg m⁻³, less than

275 10% of the measurement ($\sim 153.5 \mu\text{g m}^{-3}$). These discrepancies are likely due to the
276 biases in the uncertainties in emission inventory and small-scale dynamical fields.
277 During the period of Jan 17th to Jan 20th, the observed wind speed concentrates in the
278 range of 1 - 2 m s^{-1} , with an average of 1.3 m s^{-1} , while the simulated wind speed is
279 obviously higher, with an average of 2.0 m s^{-1} (Figure S4c). The observed prevailing
280 wind is northerly wind while the simulated prevails easterly wind (Figure S4d). Figure
281 S5a shows that $\text{PM}_{2.5}$ concentration is lower in the north to the Sichuan Basin while
282 higher to in the east to the basin. Therefore, the overestimated $\text{PM}_{2.5}$ concentration is
283 mainly caused by the departure of winds, which results in a false transport from the east
284 to the basin. This is also shown by the overestimation of CO concentration because the
285 observed northerly wind is not well simulated due to the complicated topography.

286

287 **4.2 Change in winter $\text{PM}_{2.5}$ concentration over the basin**

288

289 To examine impacts of a warming plateau on $\text{PM}_{2.5}$ concentration in winter in the basin,
290 we set three levels of temperature increase of 0.5°C, 1.0°C and 2.0°C over the plateau.
291 Time series of $\text{PM}_{2.5}$ concentrations in these simulations (with and without the
292 warming over the plateau) are respectively calculated. The results show that $\text{PM}_{2.5}$
293 concentration in the basin is significantly reduced (Figure 5). In comparison with three
294 levels of temperature increase, the maximal reduction occurs in the case of 2°C
295 warming, with an average of 25.1 $\mu\text{g m}^{-3}$ ($p < 0.001$). Under the circumstance of the
296 2°C warming, the maximal hourly reduction reaches to 84.6 $\mu\text{g m}^{-3}$ (Figure S6a) and
297 the maximal percentage reduction is about 64.4% (Figure S6b). We also calculate the
298 changes in $\text{PM}_{2.5}$ concentration and its percentage under the influence of the 2°C
299 warming on the basis of January 2018 (Figure S7), of which the result is consistent
300 with Figure S6, though there must inevitably be some differences in the magnitude.
301 Interestingly, the maximal reduction always occurs while $\text{PM}_{2.5}$ concentration reaches
302 a peak value, which suggests that the impact of the warming plateau is extremely

303 significant during the period of high PM_{2.5} concentration. This result is similar to
304 previous studies which also point out that extreme weather plays important roles in
305 affecting air quality (De Sario et al., 2013; Hong et al., 2019; Tsangari et al., 2016;
306 Zhang et al., 2016). That is to say, the impact of the warming plateau on air quality is
307 apt to be amplified in extremely high PM_{2.5} concentrations.

308

309 To better understand the impact of a warming plateau on PM_{2.5} concentration, we also
310 calculate changes in PM_{2.5} chemical composition in the basin. Both primary and
311 secondary aerosols in PM_{2.5} decreases more significantly with an increase in
312 temperature increment (Figure 6), except for the nitrate due to its competition for
313 ammonia with sulfate (Feng et al., 2018). As a result, the more sulfate is reduced under
314 the case of the 2°C warming, the less nitrate is reduced. As shown in Figure 6, the
315 warmer the plateau is, the more PM_{2.5} concentration and its chemical composition in
316 the basin decrease, suggesting that a warming plateau has increasing implications for
317 air quality in the basin. Here we show that the maximal impact of the plateau under
318 the case of the 2°C warming, in which secondary aerosol reduces by 19.7 $\mu\text{g m}^{-3}$,
319 accounting for 78.5% of the total reduction, greatly larger than the reduction of primary
320 aerosol. For example, the largest reduction is SOA, reducing from 23.2 $\mu\text{g m}^{-3}$ in the
321 base case to 10.8 $\mu\text{g m}^{-3}$ in the 2°C warming case. The second reduction is sulfate
322 (from 31.8 $\mu\text{g m}^{-3}$ to 28.6 $\mu\text{g m}^{-3}$). The next are nitrate and ammonium (22.3 $\mu\text{g m}^{-3}$
323 and 19.1 $\mu\text{g m}^{-3}$ in the base case, and 20.2 $\mu\text{g m}^{-3}$ and 17.5 $\mu\text{g m}^{-3}$ in the 2°C warming
324 case). Significance testing of the difference in every chemical composition between
325 the baseline simulation and the 2°C warming case is also given in Table S2. The *p*-
326 values of most chemical composition in PM_{2.5} are far less than 0.001 except that the
327 *p*-value of EC is 0.0011 (Table S2), implying for an extremely significant reduction of
328 every chemical composition in PM_{2.5} within the basin when the plateau warms by 2°C.
329 Thus, we emphasize the impact of the 2°C warming over the plateau on PM_{2.5}
330 concentration in the basin in our study. Meanwhile, we analyze the case for the 2017-

331 2018 winter, in which a similar change in PM_{2.5} chemical composition is obtained
332 when the plateau becomes 2°C warmer (Figure S8).

333

334 There are also significant changes in the spatial distribution of PM_{2.5} concentration.
335 Figure 7 shows the spatial distribution of changes in surface PM_{2.5} concentration and
336 winds after 2°C warming over the plateau. Apparently, there is a larger decrease in
337 PM_{2.5} concentration in the whole basin, and the maximal reduction is more than 30 μg
338 m⁻³. By contrast, PM_{2.5} concentration increases by 5 - 15 μg m⁻³ at the eastern edge of
339 the plateau. Wind patterns show that easterly winds over the basin enhance while
340 westerly wind over the plateau weaken (Figure S5 and Figure 7). Enhanced easterly
341 winds and weakened westerly winds are both in favor of the east-to-west transport of
342 pollutants from the basin to the plateau. We also show changes in PM_{2.5} concentration
343 and winds under the cases of 0.5°C and 1.0°C warming in January 2014, consistent
344 with the result of the 2°C warming, except that the reduction of PM_{2.5} concentration
345 and the change in wind speed are fewer (Figure S9a and Figure S9e). The case in
346 January 2018 (Figure S10a) is also similar to the result of the 2°C warming.

347

348 We further compare the difference in the surface pressure between the baseline and
349 sensitivity simulations, and find out that surface pressure over the plateau and the basin
350 all decreases when the plateau warms (Figure 8a and 8b). Over the plateau, the pressure
351 drop has a decrease characteristic from west to east (Figure 8c, Figure S9b and Figure
352 S9f, Figure S10b), which results in a decreased pressure gradient and a weakened
353 westerly wind. While in the basin, the pressure drop is less than the plateau. This leads
354 to an increased pressure gradient from the basin to the plateau, inducing an intensified
355 easterly wind. The enhanced easterly wind causes an increased transport of PM_{2.5} from
356 the basin to the plateau. On the other hand, the weakened westerly wind and the
357 enhanced easterly wind are convergent at the border between the plateau and the basin
358 (Figure 7, Figure S9a and Figure S9e, Figure S10a), jointly leading to an increase in

359 PM_{2.5} concentration at the eastern edge of the plateau. Additionally, northerly winds
360 over the basin slightly enhance, conducive to diluting the air and reducing PM_{2.5}
361 concentration. Both easterly winds transport and northerly winds dilution are favorable
362 for a reduction of PM_{2.5} concentration in the basin. In addition to the wind effect, there
363 are also other important factors to produce the PM_{2.5} reduction in the basin, such as the
364 PBLH and RH, which will be analyzed as follows.

365

366 **4.3 Impact of PBLH on PM_{2.5} concentration**

367

368 Previous studies show that the PBL development plays an important role in diffusing
369 pollutants (Miao et al., 2017; Su et al., 2018; Tie et al., 2015). Here we calculate the
370 change in the PBLH due to the 2°C warming over the plateau, and then analyze the
371 effect of the change in PBLH on PM_{2.5} concentration in the basin.

372

373 Our results suggest that the warming plateau plays different roles in the PBL
374 development over the plateau and the basin. Due to the warming, the PBLH decreases
375 in most areas of the plateau, but it increases over the basin (Figure 9, Figure S9c and
376 Figure S9g, Figure S10c). The maximal rise occurs under the case of the 2°C warming,
377 by 50 - 200 m over the basin (Figure 9 and Figure S10c). As known, a shallow PBL
378 constrains PM_{2.5} near the surface via suppressing vertical dispersion (Fan et al., 2011;
379 Iversen, 1984). Conversely, a deep PBL is favorable for PM_{2.5} diffusion. Thus, we
380 explore the underlying cause that leads to the difference in the PBLH in the domain.
381 The PBLH is strongly related to the changes in vertical temperature and wind, Figure
382 10 and Figures S11-12 display vertical profiles of changes in temperature and winds in
383 the plateau and the basin. Results show that the warming causes a maximal warm layer
384 around 1 km above the ground of the plateau. Noticeably, the warm layer acts as a dome
385 covering 4.5 km above the Sichuan Basin (Figure 10a, Figure S11a and Figure S11c,
386 Figure S12a). Xu et al. (2017) also finds out a significant warm plume extending from

387 the plateau to the downstream Sichuan Basin and Yangtze River Delta by use of
388 NCEP/NCAR reanalysis data. We suggest that this is probably due to a sharp
389 topography decrease (from ~ 5 km in the plateau to < 1 km in the basin) which leads to
390 a warm plume via subsidence. In the basin, there is a decrease in the temperature from
391 the lower troposphere to ~ 4 km, with a maximal temperature reduction ($0.5 - 2^\circ\text{C}$)
392 located at 1.5 km to 3 km above the ground (Figure 10a, Figure S11a and Figure S11c,
393 Figure S12a). We speculate that changes in the surface pressure can account for the
394 maximal temperature reduction here. After the warming, surface pressure decreases in
395 the basin (Figure 8, Figure S9b and Figure S9f, Figure S10b), which produces more
396 convergent airflow (as shown in Figure 7, Figure S9a and Figure S9e, Figure S10a).
397 The strengthened convergent airflow induces an intensified ascending motion,
398 conducive to a reduction of temperature in the basin. As a result, the zone where the
399 maximal temperature drop appears, overlaps with the zone with the maximal ascending
400 motion. Furthermore, the intensified updraft increases the vertical temperature gradient
401 and the instability in the lower troposphere of the basin, thereby causing a higher PBLH
402 than that in the non-warming case (Figure 10b, Figure S11b and Figure S11d, Figure
403 S12b). On the contrary, the change in vertical temperature profile leads to a decreased
404 vertical temperature gradient and increased thermal stability in the lower troposphere
405 of the plateau, in which the PBLH decreases.

406

407 On the other hand, the convergent airflows by a weakened westerly wind over the
408 plateau and a strengthened easterly wind in the basin triggers an ascending motion on
409 the east side of the plateau (Figure 10a, Figure S11a and Figure S11c, Figure S12a),
410 which is also beneficial to the development of the PBLH in the basin. Consequently,
411 the elevated PBL facilitates vertical diffusion, leading to a reduction in $\text{PM}_{2.5}$
412 concentration over the basin.

413

414 **4.4 Effect of RH on $\text{PM}_{2.5}$ concentration**

415

416 In addition to the PBLH, ambient RH is a key factor for secondary aerosol formation
417 (Tie et al., 2017; Wang et al., 2016). Previous studies indicate that aerosol hygroscopic
418 growth cannot occur until the humidity exceeds 50% (Liu et al., 2008). When the
419 humidity is greater than 60%, hygroscopic growth factor of urban aerosol increases
420 significantly with humidity (Liu et al., 2008).

421

422 We examine the influence of the RH change induced by a warming plateau on PM_{2.5}
423 concentration in the basin. Results show that there is remarkable change in RH in the
424 basin due to the warming of the plateau (Figure 11, Figure S9d and Figure S9h, Figure
425 S10d). In the baseline simulation, the RH varies in the range of 40% - 80% over the
426 basin (Figure 11a). However, the RH varies from 50% to 70% in the 2 °C warming
427 simulation (Figure 11b), suggesting that the basin becomes drier when the plateau is
428 warmer.

429

430 The RH comparison between these numerical simulations reveals that the warming
431 causes a decrease in the RH within the basin (Figure 11c, Figure S9d and Figure S9h,
432 Figure S10d). These changes in RH have critical effects on the secondary aerosol
433 formation. As explained by Tie et al. (2017), the reduction of RH (especially during the
434 stage of RH from 80% to 70%) causes a significant decrease of hygroscopic growth on
435 the aerosol surface, resulting in less water surface for producing secondary aerosol,
436 such as sulfate and nitrate. As a result, PM_{2.5} concentration decreases in the basin. There
437 are also some fingerprints of the RH's effect on PM_{2.5} concentration. Firstly, the spatial
438 distributions of RH reduction and PM_{2.5} concentration reduction have similar patterns
439 (Figure 11c and Figure 7, Figure S9a and Figure S9d, Figure S9e and Figure S9h, Figure
440 S10a and Figure S10d), and the region with more humidity decrease overlaps the region
441 with more PM_{2.5} decreases. Secondly, as shown in Figure 6, the changes in PM_{2.5}
442 compositions indicate that the reduced PM_{2.5} concentration is mainly caused by the
443 decrease in secondary aerosol concentration. Therefore, the RH change also plays an

444 important role for PM_{2.5} concentration in the basin.

445

446 **5 Conclusions**

447

448 ERA-interim reanalysis data and observation records at 10 weather stations show that
449 the Tibetan Plateau is significantly warming during the past four decades (1979-2017),
450 particularly in winter. The temperature increase rate is 0.5°C decade⁻¹ to 1.0°C decade⁻¹
451 ¹ in winter, approximately twice as much as the increase rate of annual mean
452 temperature. In recent 5 years (2013-2017), the central plateau is significantly warming
453 with an increase rate of 1.0°C yr⁻¹, encompassing the warming rate during the entire 40
454 years. Rapid warming has caused the winter temperature to increase by an average of
455 2°C over the entire plateau from 2013 to 2017.

456

457 The WRF-Chem model is used to assess the impact of a warming plateau on air quality
458 over the downstream Sichuan Basin. The most significant impact of the plateau on
459 PM_{2.5} concentration in the basin occurs under the case of the 2°C warming. Through an
460 enhanced horizontal transport, a reduced RH and an increased PBLH, the warming
461 plateau significantly reduces PM_{2.5} concentration in the basin. A larger pressure
462 gradient from the basin to the plateau is favorable for an east-to-west transport for
463 pollutants within the basin. A lower ambient RH decreases aerosol hygroscopic growth,
464 which weakens secondary aerosol formation and leads to a significant reduction in
465 secondary aerosol concentration. Moreover, the warming induces an increase in vertical
466 temperature gradient over the basin, strengthening turbulence mixing and elevating
467 PBLH. The elevated PBLH is favorable for vertical diffusion that causes a reduction of
468 PM_{2.5} in the basin. Additionally, the uplift effect by an enhanced ascending motion at
469 the eastern edge of the plateau also contributes to PM_{2.5} reduction within the basin.

470

471 In summary, the warming over the plateau in recent five years comprehensively induces

472 a rising PBLH and a drying ambient air over the basin, which greatly reduces PM_{2.5}
473 secondary compositions. On average, PM_{2.5} concentration reduces by 25.1 μg m⁻³ on
474 the basis of the 2013-2014 winter, of which the primary and secondary aerosols
475 decrease by 5.4 μg m⁻³ and 19.7 μg m⁻³, respectively. Here we need to clarify that our
476 model domain may be a little small to comprehensively atmospheric circulation pattern
477 related to the Tibetan Plateau and the subsequent impact on air quality in the basin,
478 though the domain covers almost the whole plateau and the basin. We notice that the
479 basin is nearby the eastern boundary of the domain, in which local circulation might be
480 influenced by the lateral condition. Therefore, as the plateau is likely to continue
481 warming, in-depth understanding to climate change on the Tibetan Plateau and long-
482 term PM_{2.5} measurements are required to validate the impact of the warming plateau on
483 air quality in a larger spatial scale.

484

485 *Data availability.* The data used in this study are available from the corresponding
486 author upon request (tiexx@ieecas.cn).

487 *Supplement.* Supplemental materials to this article can be found online at <http://xxxxxxx>

488 *Author contributions.* XX designed research, and revised the final paper. SY performed
489 research, and wrote the paper. XX and SY provided financial support. TF validated the
490 model, modified the chart code and reviewed the paper. ZB collected and analyzed the
491 weather-stations data.

492 *Competing interests.* The authors declare that they have no conflict of interest.

493 *Acknowledgements.* This work is supported by the National Natural Science Foundation
494 of China (Nos. 41430424, 41730108 and 41807307) and the West Light Foundation of
495 the Chinese Academy of Sciences (Nos. XAB2016B04). We also would like to
496 acknowledge European Center for Medium-Range Weather Forecasts (ERA-interim)
497 for reanalysis data which are freely obtained by a following registration on the website
498 <http://apps.ecmwf.int/datasets/>. Ambient weather-station observations are obtained
499 from the National Oceanic and Atmospheric Administration (NOAA),
500 <http://gis.ncdc.noaa.gov/map/viewer/#app=clim&cfg=cdo&theme=hourly&layers=1>
501 &node=gis. The hourly ambient surface O₃, CO and PM_{2.5} mass concentrations are real-
502 timely released by Ministry of Environmental Protection, China on the website

503 <http://www.aqistudy.cn/>, freely downloaded from <http://106.37.208.233:20035/>. The
504 MEIC-2012 (Multi-resolution Emission Inventory for China) anthropogenic emission
505 inventory is available on the website, <http://www.meicmodel.org>. The authors also
506 thank anonymous reviewers for their helpful comments and suggestions.

507 **Reference**

508

509 Bei, N., Li, G., Huang, R.-J., Cao, J., Meng, N., Feng, T., Liu, S., Zhang, T., Zhang, Q.
510 and Molina, L. T.: Typical synoptic situations and their impacts on the wintertime air
511 pollution in the Guanzhong basin, China, *Atmos. Chem. Phys.*, 16(11), 7373–7387,
512 doi:10.5194/acp-16-7373-2016, 2016.

513 Bei, N., Zhao, L., Xiao, B., Meng, N. and Feng, T.: Impacts of local circulations on the
514 wintertime air pollution in the Guanzhong Basin, China, *Science of The Total
515 Environment*, 592, 373–390, doi:10.1016/j.scitotenv.2017.02.151, 2017.

516 Binkowski, F. S.: Models-3 Community Multiscale Air Quality (CMAQ) model aerosol
517 component 1. Model description, *J. Geophys. Res.*, 108(D6), 2981,
518 doi:10.1029/2001JD001409, 2003.

519 Cai, W., Li, K., Liao, H., Wang, H. and Wu, L.: Weather conditions conducive to Beijing
520 severe haze more frequent under climate change, *Nat. Clim. Change*, 7(4), 257–262,
521 doi:10.1038/nclimate3249, 2017.

522 Chen, F. and Dudhia, J.: Coupling an Advanced Land Surface–Hydrology Model with
523 the Penn State–NCAR MM5 Modeling System. Part I: Model Implementation and
524 Sensitivity, *Mon. Weather Rev.*, 129(4), 569–585, doi:10.1175/1520-
525 0493(2001)129<0569:CAALSH>2.0.CO;2, 2001.

526 De Sario, M., Katsouyanni, K. and Michelozzi, P.: Climate change, extreme weather
527 events, air pollution and respiratory health in Europe, *Eur Respir J*, 42(3), 826–843,
528 doi:10.1183/09031936.00074712, 2013.

529 Duan, A., Wu, G., Liu, Y., Ma, Y. and Zhao, P.: Weather and climate effects of the
530 Tibetan Plateau, *Adv. in Atmos. Sci.*, 29(5), 978–992, doi:10.1007/s00376-012-1220-y,
531 2012.

532 Dudhia, J.: Numerical Study of Convection Observed during the Winter Monsoon
533 Experiment Using a Mesoscale Two-Dimensional Model, *J. Atmos. Sci.*, 46(20), 3077–
534 3107, doi:10.1175/1520-0469(1989)046<3077:NSOCOD>2.0.CO;2, 1989.

535 Emmons, L. K., Walters, S., Hess, P. G., Lamarque, J. F., Pfister, G. G., Fillmore, D.,
536 Granier, C., Guenther, A., Kinnison, D., Laepple, T., Orlando, J., Tie, X., Tyndall, G.,

537 Wiedinmyer, C., Baughcum, S. L. and Kloster, S.: Description and evaluation of the
538 Model for Ozone and Related chemical Tracers, version 4 (MOZART-4), *Geosci.*
539 *Model Dev.*, 3(1), 43–67, doi:10.5194/gmd-3-43-2010, 2010.

540 Fan, S. J., Fan, Q., Yu, W., Luo, X. Y., Wang, B. M., Song, L. L. and Leong, K. L.:
541 Atmospheric boundary layer characteristics over the Pearl River Delta, China, during
542 the summer of 2006: measurement and model results, *Atmos. Chem. Phys.*, 11(13),
543 6297–6310, doi:10.5194/acp-11-6297-2011, 2011.

544 Feng, T., Bei, N., Zhao, S., Wu, J., Li, X., Zhang, T., Cao, J., Zhou, W. and Li, G.:
545 Wintertime nitrate formation during haze days in the Guanzhong basin, China: A case
546 study, *Environmental Pollution*, 243(Part B), 1057–1067,
547 doi:10.1016/j.envpol.2018.09.069, 2018.

548 Feng, T., Li, G., Cao, J., Bei, N., Shen, Z., Zhou, W., Liu, S., Zhang, T., Wang, Y., Huang,
549 R.-J., Tie, X. and Molina, L. T.: Simulations of organic aerosol concentrations during
550 springtime in the Guanzhong Basin, China, *Atmos. Chem. Phys.*, 16(15), 10045–10061,
551 doi:10.5194/acp-16-10045-2016, 2016.

552 Grell, G. A., Peckham, S. E., Schmitz, R., McKeen, S. A., Frost, G., Skamarock, W. C.
553 and Eder, B.: Fully coupled “online” chemistry within the WRF model, *Atmos.*
554 *Environ.*, 39(37), 6957–6975, doi:10.1016/j.atmosenv.2005.04.027, 2005.

555 Guenther, A., Karl, T., Harley, P., Wiedinmyer, C., Palmer, P. I. and Geron, C.: Estimates
556 of global terrestrial isoprene emissions using MEGAN (Model of Emissions of Gases
557 and Aerosols from Nature), *Atmos. Chem. Phys.*, 6(11), 3181–3210, doi:10.5194/acp-
558 6-3181-2006, 2006.

559 Hong, C., Zhang, Q., Zhang, Y., Davis, S. J., Tong, D., Zheng, Y., Liu, Z., Guan, D., He,
560 K. and Schellnhuber, H. J.: Impacts of climate change on future air quality and human
561 health in China, *P. Natl. Acad. Sci. USA*, 116(35), 17193–17200,
562 doi:10.1073/pnas.1812881116, 2019.

563 Hong, S.-Y. and Lim, J.-O. J.: The WRF single-moment 6-class microphysics scheme
564 (WSM6), *J. Korean Meteor. Soc.*, 42(2), 129–151, 2006.

565 Hua, M.: Analysis and simulation study on the influence of heat condition over
566 Qinghai-Xizang Plateau on climate over South-West China, *Plateau Meteorology*, 22,
567 152–156, 2017.

568 Iversen, T.: On the atmospheric transport of pollution to the Arctic, *Geophys. Res. Lett.*,
569 11(5), 457–460, doi:10.1029/GL011i005p00457, 1984.

570 Janjić, Z. I.: Nonsingular implementation of the Mellor-Yamada level 2.5 scheme in the
571 NCEP meso model, Camp Springs, MD. 2002.

572 Kuang, X. and Jiao, J. J.: Review on climate change on the Tibetan Plateau during the
573 last half century, *J. Geophys. Res.*, 1–29, doi:10.1002/(ISSN)2169-8996, 2016.

574 Li, G., Bei, N., Cao, J., Huang, R., Wu, J., Feng, T., Wang, Y., Liu, S., Zhang, Q., Tie,
575 X. and Molina, L. T.: A possible pathway for rapid growth of sulfate during haze days
576 in China, *Atmos. Chem. Phys.*, 17(5), 3301–3316, doi:10.5194/acp-17-3301-2017,
577 2017a.

578 Li, G., Bei, N., Tie, X. and Molina, L. T.: Aerosol effects on the photochemistry in
579 Mexico City during MCMA-2006/MILAGRO campaign, *Atmos. Chem. Phys.*, 11(11),
580 5169–5182, doi:10.5194/acp-11-5169-2011, 2011a.

581 Li, G., Lei, W., Zavala, M., Volkamer, R., Dusanter, S., Stevens, P. and Molina, L. T.:
582 Impacts of HONO sources on the photochemistry in Mexico City during the MCMA-
583 2006/MILAGO Campaign, *Atmos. Chem. Phys.*, 10(14), 6551–6567, doi:10.5194/acp-
584 10-6551-2010, 2010.

585 Li, G., Zavala, M., Lei, W., Tsimpidi, A. P., Karydis, V. A., Pandis, S. N., Canagaratna,
586 M. R. and Molina, L. T.: Simulations of organic aerosol concentrations in Mexico City
587 using the WRF-CHEM model during the MCMA-2006/MILAGRO campaign, *Atmos.*
588 *Chem. Phys.*, 11(8), 3789–3809, doi:10.5194/acp-11-3789-2011, 2011b.

589 Li, M., Zhang, Q., Kurokawa, J.-I., Woo, J.-H., He, K., Lu, Z., Ohara, T., Song, Y.,
590 Streets, D. G., Carmichael, G. R., Cheng, Y., Hong, C., Huo, H., Jiang, X., Kang, S.,
591 Liu, F., Su, H. and Zheng, B.: MIX: a mosaic Asian anthropogenic emission inventory
592 under the international collaboration framework of the MICS-Asia and HTAP, *Atmos.*
593 *Chem. Phys.*, 17(2), 935–963, doi:10.5194/acp-17-935-2017, 2017b.

594 Liu, X. and Chen, B.: CLIMATIC WARMING IN THE TIBETAN PLATEAU
595 DURING RECENT DECADES, *Int. J. Climatol.*, 20, 1729–1742, 2000.

596 Liu, X., Cheng, Y., Zhang, Y., Jung, J., Sugimoto, N., Chang, S.-Y., Kim, Y. J., Fan, S.
597 and Zeng, L.: Influences of relative humidity and particle chemical composition on
598 aerosol scattering properties during the 2006 PRD campaign, *Atmos. Environ.*, 42(7),
599 1525–1536, doi:10.1016/j.atmosenv.2007.10.077, 2008.

600 Miao, Y., Guo, J., Liu, S., Liu, H., Li, Z., Zhang, W. and Zhai, P.: Classification of
601 summertime synoptic patterns in Beijing and their associations with boundary layer
602 structure affecting aerosol pollution, *Atmos. Chem. Phys.*, 17(4), 3097–3110,
603 doi:10.5194/acp-17-3097-2017, 2017.

604 Qiao, X., Guo, H., Tang, Y., Wang, P., Deng, W., Zhao, X., Hu, J., Ying, Q. and Zhang,
605 H.: Local and regional contributions to fine particulate matter in the 18 cities of Sichuan
606 Basin, southwestern China, *Atmos. Chem. Phys.*, 19(9), 5791–5803, doi:10.5194/acp-
607 19-5791-2019, 2019.

608 Rangwala, I., Miller, J. R. and Xu, M.: Warming in the Tibetan Plateau: Possible
609 influences of the changes in surface water vapor, *Geophys. Res. Lett.*, 36(6), 5–6,
610 doi:10.1029/2009GL037245, 2009.

611 Su, T., Li, Z. and Kahn, R.: Relationships between the planetary boundary layer height
612 and surface pollutants derived from lidar observations over China: regional pattern and
613 influencing factors, *Atmos. Chem. Phys.*, 18(21), 15921–15935, doi:10.5194/acp-18-
614 15921-2018, 2018.

615 Tao, J., Zhang, L., Cao, J. and Zhang, R.: A review of current knowledge concerning
616 PM 2.5 chemical composition, aerosol optical properties and their relationships across
617 China, *Atmos. Chem. Phys.*, 17(15), 9485–9518, doi:10.5194/acp-17-9485-2017, 2017.

618 Tie, X., Huang, R.-J., Cao, J., Zhang, Q., Cheng, Y., Su, H., Di Chang, schl, U. P. X.,
619 Hoffmann, T., Dusek, U., Li, G., Worsnop, D. R. and Dowd, C. D. O. X.: Severe
620 Pollution in China Amplified by Atmospheric Moisture, *Sci. Rep.*, 1–8,
621 doi:10.1038/s41598-017-15909-1, 2017.

622 Tie, X., Madronich, S., Li, G., Ying, Z., Weinheimer, A., Apel, E. and Campos, T.:
623 Simulation of Mexico City plumes during the MIRAGE-Mex field campaign using the
624 WRF-Chem model, *Atmos. Chem. Phys.*, 9(14), 4621–4638, doi:10.5194/acp-9-4621-
625 2009, 2009.

626 Tie, X., Madronich, S., Li, G., Ying, Z., Zhang, R., Garcia, A. R., Lee-Taylor, J. and
627 Liu, Y.: Characterizations of chemical oxidants in Mexico City: A regional chemical
628 dynamical model (WRF-Chem) study, *Atmos. Environ.*, 41(9), 1989–2008,
629 doi:10.1016/j.atmosenv.2006.10.053, 2007.

630 Tie, X., Madronich, S., Walters, S., Zhang, R., Rasch, P. and Collins, W.: Effect of
631 clouds on photolysis and oxidants in the troposphere, *J. Geophys. Res.*, 108(D20), 4642,
632 doi:10.1029/2003JD003659, 2003.

633 Tie, X., Sasha, M., Stacy, W., David, E., Paul, G., Natalie, M., Renyi, Z., Lou, C. and
634 Guy, B.: Assessment of the global impact of aerosols on tropospheric oxidants, *J.*
635 *Geophys. Res.*, 110(D03204), 13,791, doi:10.1029/2004JD005359, 2005.

636 Tie, X., Zhang, Q., He, H., Cao, J., Han, S., Gao, Y., Li, X. and Jia, X. C.: A budget
637 analysis of the formation of haze in Beijing, *Atmos. Environ.*, 100, 25–36,
638 doi:10.1016/j.atmosenv.2014.10.038, 2015.

639 Tsangari, H., Paschalidou, A. K., Kassomenos, A. P., Vardoulakis, S., Heaviside, C.,
640 Georgiou, K. E. and Yamasaki, E. N.: Extreme weather and air pollution effects on
641 cardiovascular and respiratory hospital admissions in Cyprus, *Science of The Total*
642 *Environment*, 542(Part A), 247–253, doi:10.1016/j.scitotenv.2015.10.106, 2016.

- 643 Wang, G., Zhang, R., Gomez, M. E., Yang, L., Levy Zamora, M., Hu, M., Lin, Y., Peng,
644 J., Guo, S., Meng, J., Li, J., Cheng, C., Hu, T., Ren, Y., Wang, Y., Gao, J., Cao, J., An,
645 Z., Zhou, W., Li, G., Wang, J., Tian, P., Marrero-Ortiz, W., Secretst, J., Du, Z., Zheng,
646 J., Shang, D., Zeng, L., Shao, M., Wang, W., Huang, Y., Wang, Y., Zhu, Y., Li, Y., Hu,
647 J., Pan, B., Cai, L., Cheng, Y., Ji, Y., Zhang, F., Rosenfeld, D., Liss, P. S., Duce, R. A.,
648 Kolb, C. E. and Molina, M. J.: Persistent sulfate formation from London Fog to Chinese
649 haze, *P. Natl. Acad. Sci. USA*, 113(48), 13630–13635, doi:10.1073/pnas.1616540113,
650 2016.
- 651 Wang, H., Tian, M., Chen, Y., Shi, G., Liu, Y., Yang, F., Zhang, L., Deng, L., Yu, J.,
652 Peng, C. and Cao, X.: Seasonal characteristics, formation mechanisms and source
653 origins of PM_{2.5} in two megacities in Sichuan Basin, China, *Atmos. Chem. Phys.*, 18(2),
654 865–881, doi:10.5194/acp-18-865-2018, 2018.
- 655 Wesely, M. L.: Parameterization of surface resistances to gaseous dry deposition in
656 regional-scale numerical models, *Atmospheric Environment* (1967), 23(6), 1293–1304,
657 doi:10.1016/0004-6981(89)90153-4, 1989.
- 658 Xu, J., Chang, L., Yan, F. and He, J.: Role of climate anomalies on decadal variation in
659 the occurrence of wintertime haze in the Yangtze River Delta, China, *Science of The*
660 *Total Environment*, 599-600, 918–925, doi:10.1016/j.scitotenv.2017.05.015, 2017.
- 661 Xu, X., Zhao, T., Liu, F., Gong, S. L., Kristovich, D., Lu, C., Guo, Y., Cheng, X., Wang,
662 Y. and Ding, G.: Climate modulation of the Tibetan Plateau on haze in China, *Atmos.*
663 *Chem. Phys.*, 16(3), 1365–1375, doi:10.5194/acp-16-1365-2016, 2016.
- 664 Yang, F., Tan, J., Zhao, Q., Du, Z., He, K., Ma, Y., Duan, F., Chen, G. and Zhao, Q.:
665 Characteristics of PM_{2.5} speciation in representative megacities and across China,
666 *Atmos. Chem. Phys.*, 11(11), 5207–5219, doi:10.5194/acp-11-5207-2011, 2011.
- 667 Zhang, H., Wang, Y., Park, T.-W. and Deng, Y.: Quantifying the relationship between
668 extreme air pollution events and extreme weather events, *Atmospheric Research*, 1–48,
669 doi:10.1016/j.atmosres.2016.11.010, 2016.
- 670 Zhang, Q., Streets, D. G., Carmichael, G. R., He, K. B., Huo, H., Kannari, A., Klimont,
671 Z., Park, I. S., Reddy, S., Fu, J. S., Chen, D., Duan, L., Lei, Y., Wang, L. T. and Yao, Z.
672 L.: Asian emissions in 2006 for the NASA INTEX-B mission, *Atmos. Chem. Phys.*,
673 9(14), 5131–5153, doi:10.5194/acp-9-5131-2009, 2009.
- 674 Zhao, P., Li, Y., Guo, X., Xu, X., Liu, Y., Tang, S., Xiao, W., Shi, C., Ma, Y., Yu, X.,
675 Liu, H., Jia, L., Chen, Y., Liu, Y., Li, J., Luo, D., Cao, Y., Zheng, X., Chen, J., Xiao, A.,
676 Yuan, F., Chen, D., Pang, Y., Hu, Z., Zhang, S., Dong, L., Hu, J., Han, S. and Zhou, X.:
677 The Tibetan Plateau Surface-Atmosphere Coupling System and Its Weather and
678 Climate Effects: The Third Tibetan Plateau Atmospheric Science Experiment, *J*
679 *Meteorol Res*, 33(3), 375–399, doi:10.1007/s13351-019-8602-3, 2019.

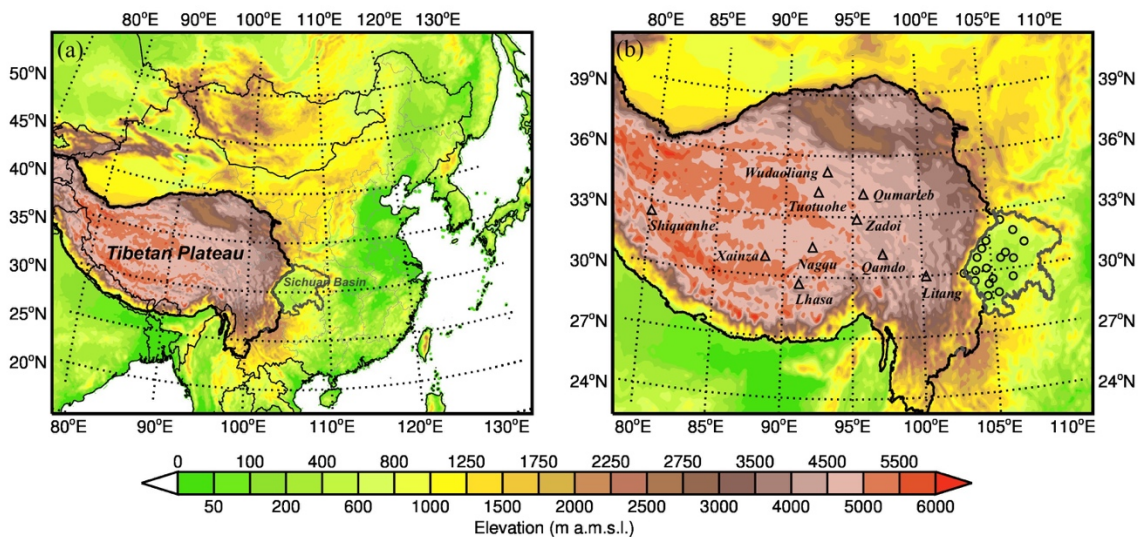
- 680 Zhao, S., Feng, T., Tie, X., Long, X., Li, G., Cao, J., Zhou, W. and An, Z.: Impact of
681 Climate Change on Siberian High and Wintertime Air Pollution in China in Past Two
682 Decades, *Earth's Future*, 6, 118–133, doi:10.1002/2017EF000682, 2018.
- 683 Zhao, S., Tie, X., Cao, J. and Zhang, Q.: Impacts of mountains on black carbon aerosol
684 under different synoptic meteorology conditions in the Guanzhong region, China,
685 *Atmospheric Research*, 164-165(C), 286–296, doi:10.1016/j.atmosres.2015.05.016,
686 2015.
- 687 Zhu, Q., Shou, S. and Tang, D.: *Principles and methods of weather*, 4 ed., Beijing. 2000.
- 688 Zou, Y., Wang, Y., Zhang, Y. and Koo, J.-H.: Arctic sea ice, Eurasia snow, and extreme
689 winter haze in China, *Sci. Adv.*, 3(3), e1602751–9, doi:10.1126/sciadv.1602751, 2017.
- 690

Figure captions

691
692
693
694
695
696
697
698
699
700
701
702
703
704
705
706
707
708
709
710
711
712
713
714
715
716
717
718
719
720
721
722
723
724
725
726
727
728
729
730
731
732
733

- Figure 1** (a) Location map of the Tibetan Plateau (the region surrounded by the dark line) and the Sichuan Basin (the region surrounded by the gray line). (b) The model domain and the distribution of weather stations marked in the triangles over the Tibetan Plateau and air quality stations marked in the circles over the Sichuan Basin.
- Figure 2** Trends of observational winter (Dec-Jan-Feb) mean temperature anomaly recorded by 10 weather stations over the Tibetan Plateau during the last four decades (1979-2017).
- Figure 3** Trends of ERA-interim reanalysis winter mean temperature over the Tibetan Plateau from 1979 to 2017. The dotted regions show statistical significance with 95% confidence level (p -value < 0.05) from the Student's t test.
- Figure 4** Comparison between the observed (black dots) and simulated (blue line) hourly O_3 ($\mu\text{g m}^{-3}$), CO (mg m^{-3}) and $PM_{2.5}$ mass concentration ($\mu\text{g m}^{-3}$) over the Sichuan Basin in January 2014.
- Figure 5** Time series of $PM_{2.5}$ concentration over the Sichuan Basin, the baseline simulation is selected in January 2014 and the sensitivity simulations in which 0.5°C , 1.0°C , and 2°C warming occur over the Tibetan Plateau relative to the baseline simulation. The differences in $PM_{2.5}$ concentrations between the baseline simulation and sensitivity simulations are significant, exceeding 99.9% confidence level ($p < 0.001$).
- Figure 6** Comparisons of $PM_{2.5}$ chemical composition in the Sichuan Basin between the baseline simulation (black) and sensitivity simulations that the plateau warms by 0.5°C (green), 1.0°C (yellow) and 2.0°C (red).
- Figure 7** Difference in spatial distributions of surface $PM_{2.5}$ concentration (shading) and winds (arrows) between the sensitivity simulation and baseline simulation. The negative shows $PM_{2.5}$ concentration decreases and the positive shows $PM_{2.5}$ concentration increases when the Tibetan Plateau is 2°C warming.
- Figure 8** Comparison of spatial distributions of sea level pressure (SLP) between the (a) baseline simulation and (b) sensitivity simulation over the Tibetan Plateau and Sichuan Basin. (c) Changes in SLPs (sensitivity simulation *minus* baseline simulation) over the plateau and basin while the plateau becomes 2°C warming.
- Figure 9** Spatial change in the PBLH induced by 2°C warming over the Tibetan Plateau. The positive shows the PBLH increases while the negative shows the PBLH decreases.
- Figure 10** Vertical profiles of changes in temperature (shading and gray contour) and winds (arrows) along 30°N in January 2014. The gray shaded area presents topography. The green box for the Sichuan Basin, and the red solid (baseline simulation) and dash (sensitivity simulation) lines for the PBLH. (a) The Tibetan Plateau and Sichuan Basin, and (b) The Sichuan Basin.
- Figure 11** Comparison of spatial distributions of RH between (a) baseline simulation and (b) sensitivity simulation over the Tibetan Plateau and Sichuan Basin. (c) Similar to Figure 9, but for RH spatial changes when the plateau becomes 2°C warming, and the positive shows the RH increases while the negative shows the RH decreases.

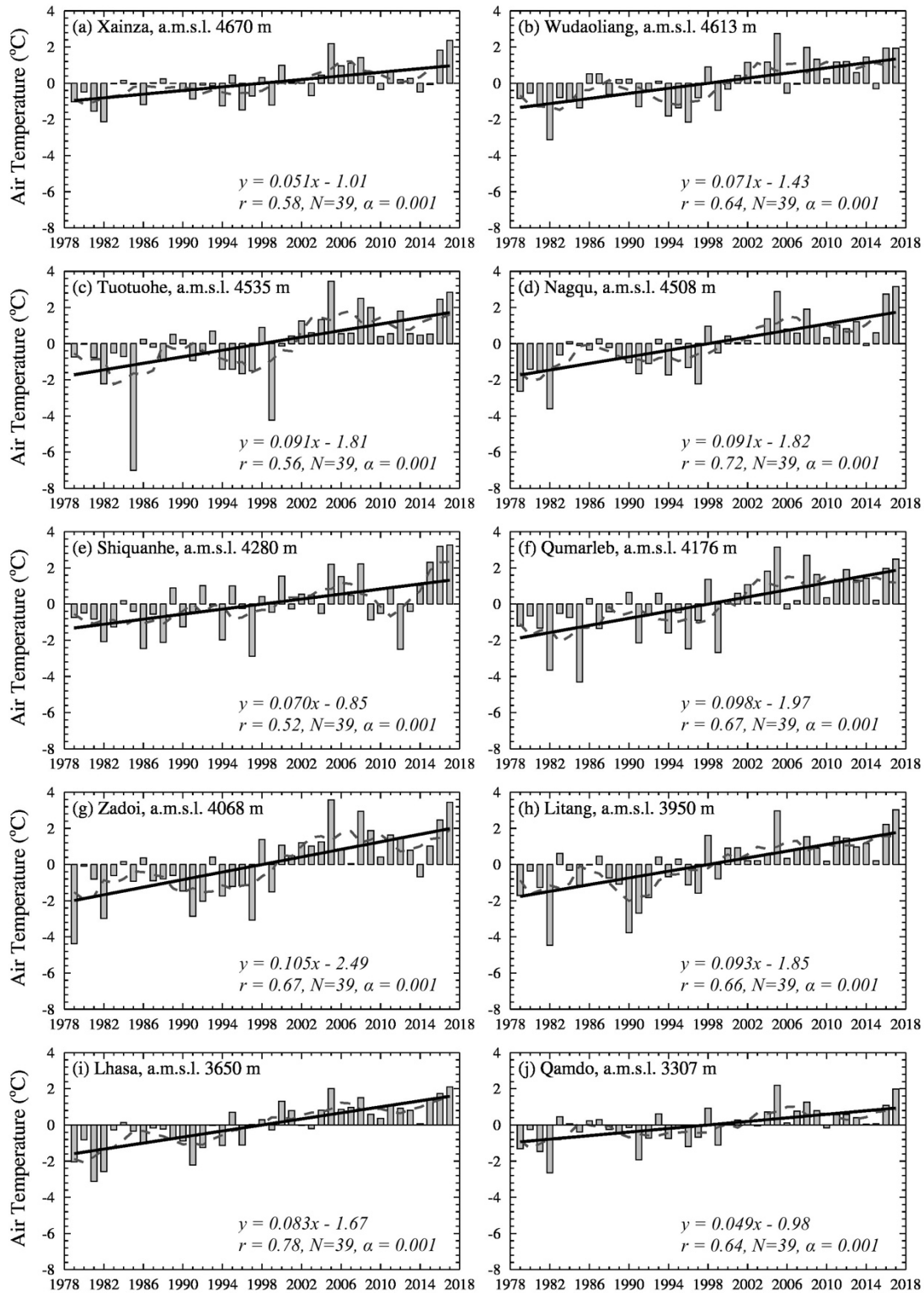
734



735

736 **Figure 1** (a) Location map of the Tibetan Plateau (the region surrounded by the dark line) and
737 the Sichuan Basin (the region surrounded by the gray line). (b) The model domain and the
738 distribution of weather stations marked in the triangles over the Tibetan Plateau and air quality
739 stations marked in the circles over the Sichuan Basin.

740



741

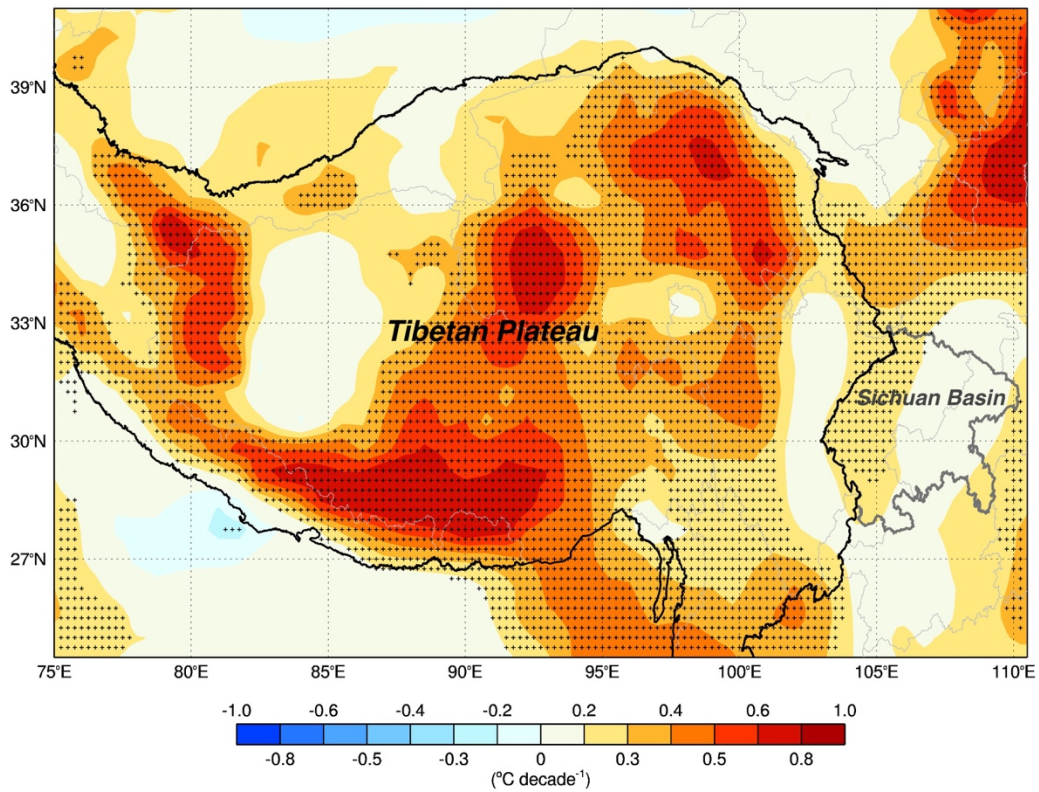
742

Figure 2 Trends of observational winter (Dec-Jan-Feb) mean temperature anomaly recorded by 10 weather stations over the Tibetan Plateau during the last four decades (1979-2017).

743

744

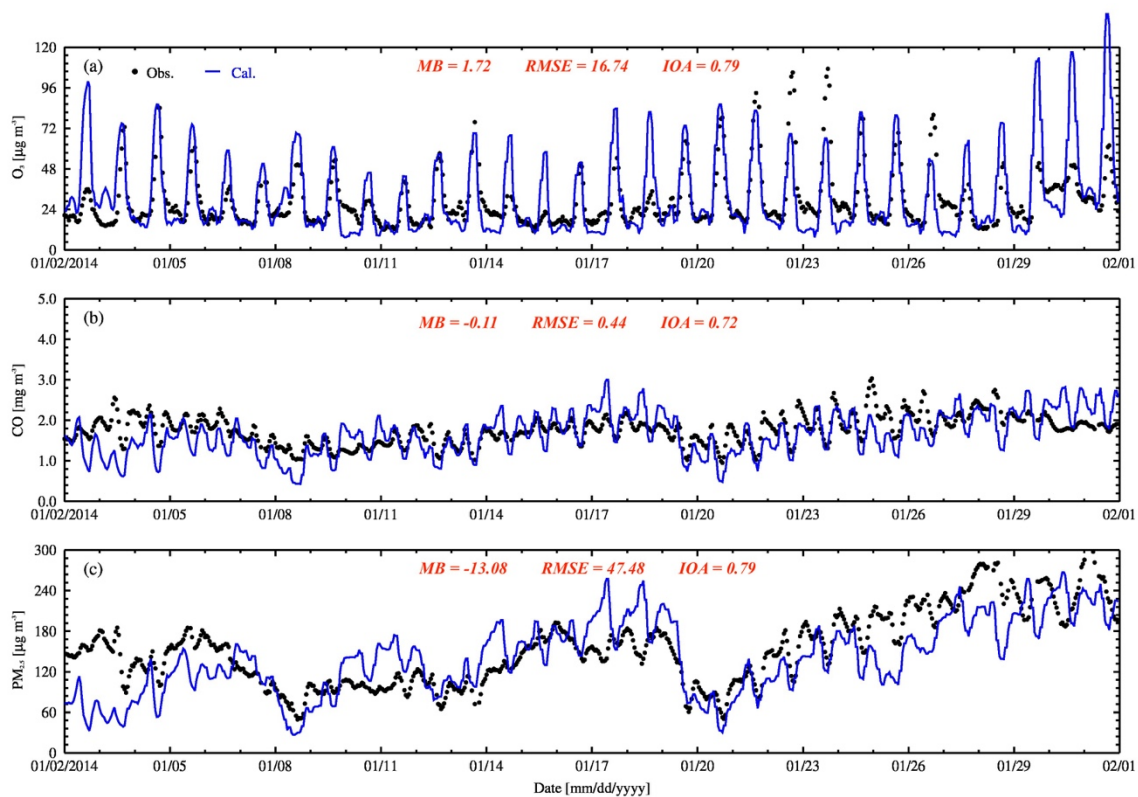
745



746

747 **Figure 3** Trends of ERA-interim reanalysis winter mean temperature over the Tibetan Plateau
748 from 1979 to 2017. The dotted regions show statistical significance with 95% confidence level
749 (p -value < 0.05) from the Student's t test.
750

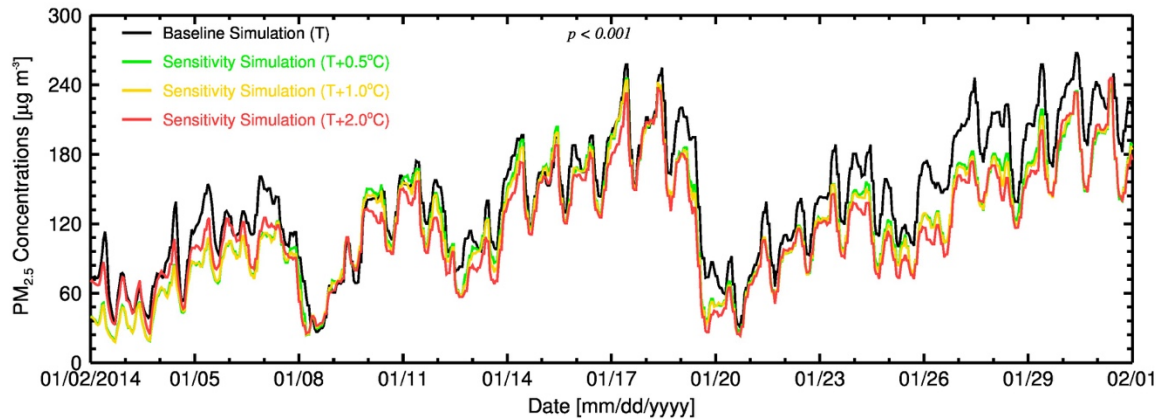
751



752

753 **Figure 4** Comparison between the observed (black dots) and simulated (blue line) hourly O_3
754 ($\mu\text{g m}^{-3}$), CO (mg m^{-3}) and $PM_{2.5}$ mass concentration ($\mu\text{g m}^{-3}$) over the Sichuan Basin in
755 January 2014.

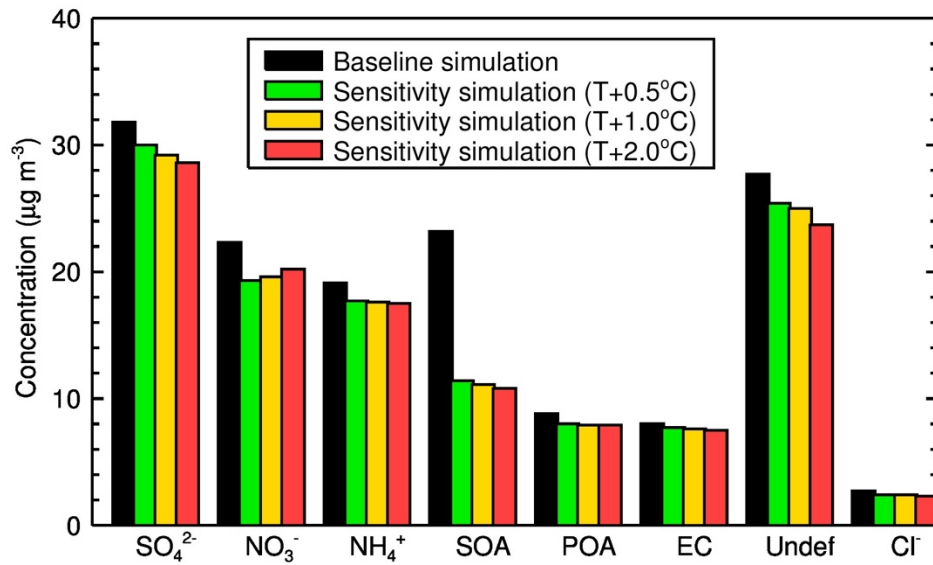
756
757



758
759
760
761
762
763
764

Figure 5 Time series of PM_{2.5} concentration over the Sichuan Basin, the baseline simulation is selected in January 2014 and the sensitivity simulations in which 0.5°C, 1.0°C, and 2°C warming occur over the Tibetan Plateau relative to the baseline simulation. The differences in PM_{2.5} concentrations between the baseline simulation and sensitivity simulations are significant, exceeding 99.9% confidence level ($p < 0.001$).

765

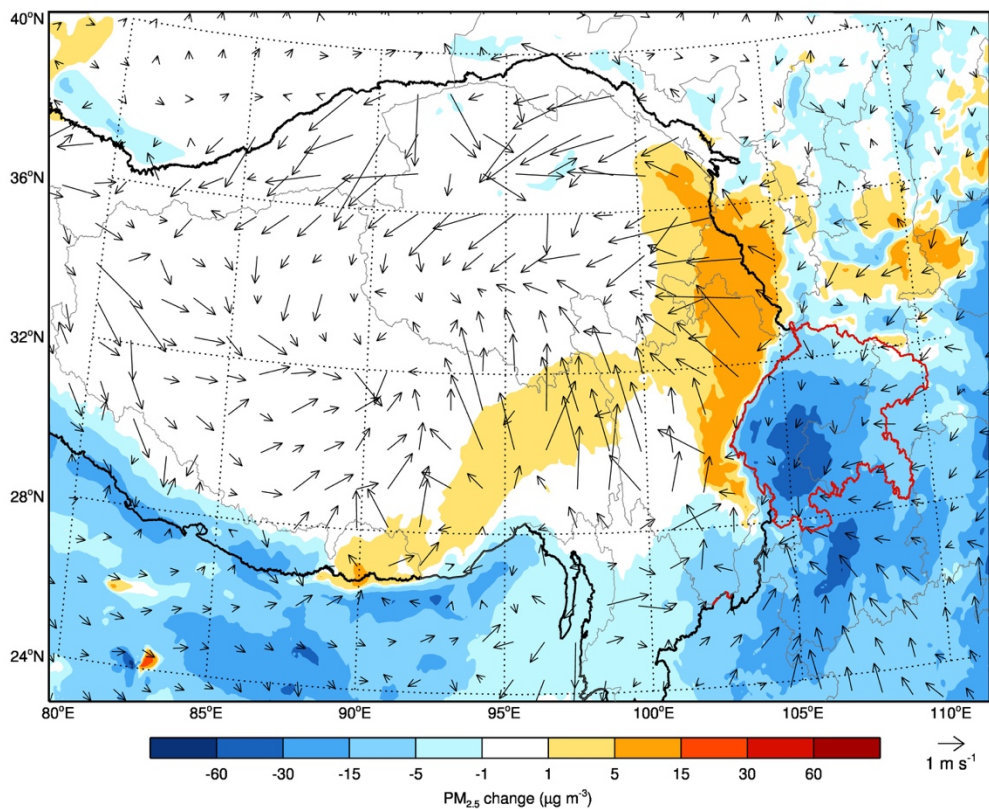


766

767 **Figure 6** Comparisons of PM_{2.5} chemical composition in the Sichuan Basin between the
768 baseline simulation (black) and sensitivity simulations that the plateau warms by 0.5°C (green),
769 1.0°C (yellow) and 2.0°C (red).

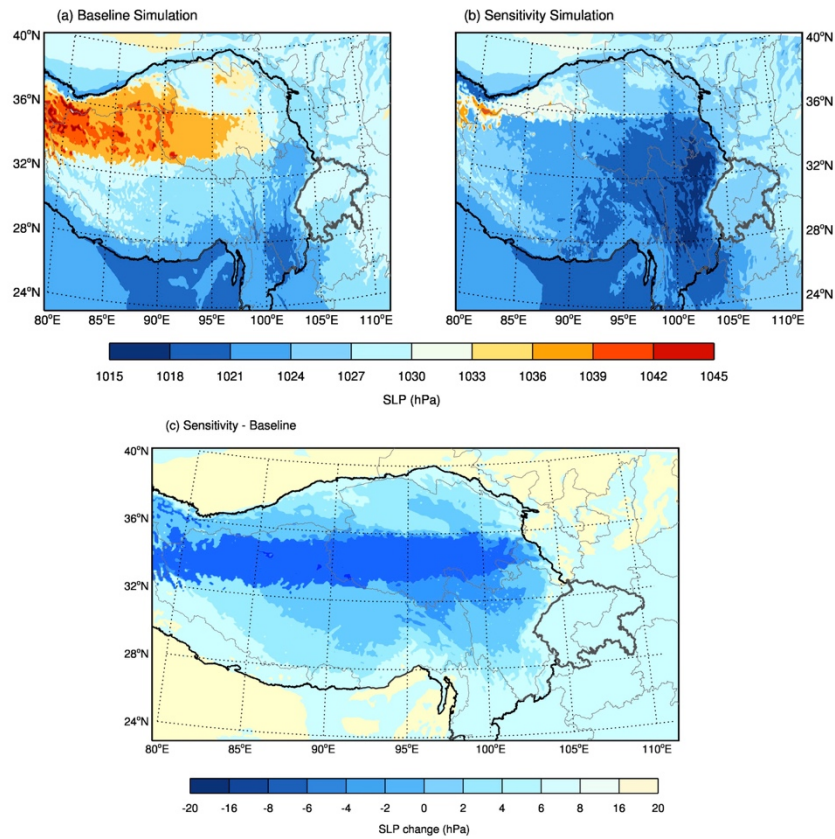
770

771



772
773
774
775
776
777

Figure 7 Difference in spatial distributions of surface PM_{2.5} concentration (shading) and winds (arrows) between the sensitivity simulation and baseline simulation. The negative shows PM_{2.5} concentration decreases and the positive shows PM_{2.5} concentration increases when the Tibetan Plateau is 2°C warming.

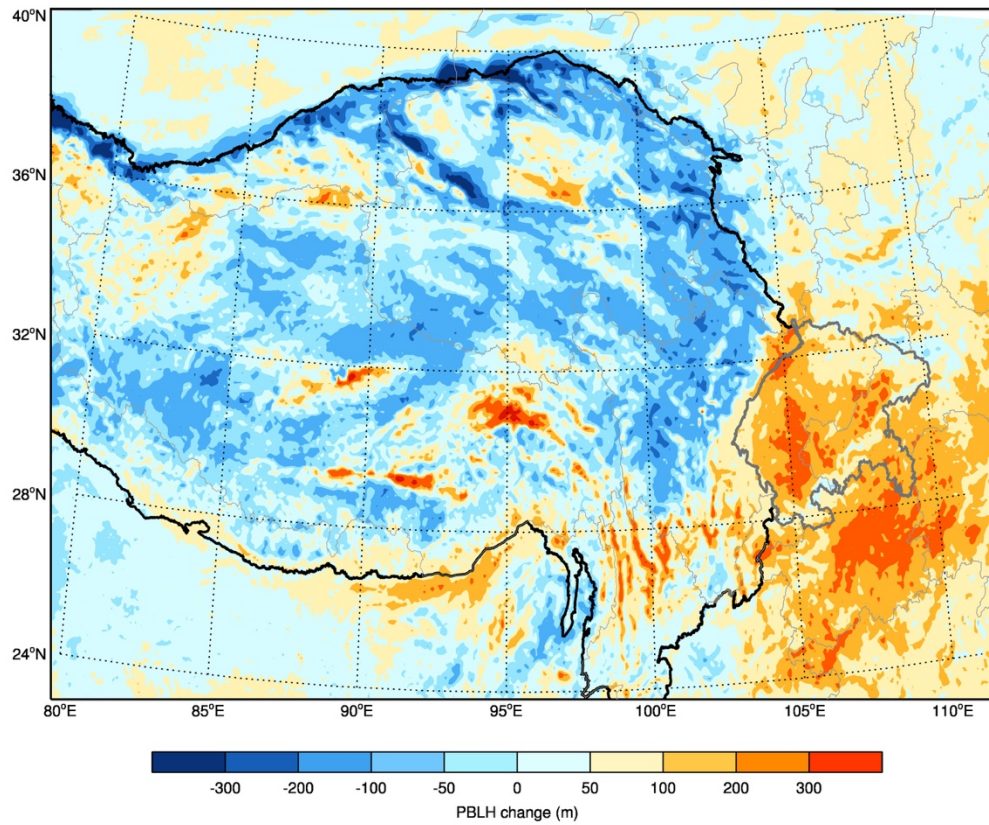


779

780 **Figure 8** Comparison of spatial distributions of sea level pressure (SLP) between the (a)
 781 baseline simulation and (b) sensitivity simulation over the Tibetan Plateau and Sichuan Basin.
 782 (c) Changes in SLPs (sensitivity simulation *minus* baseline simulation) over the plateau and
 783 basin while the plateau becomes 2°C warming.

784

785

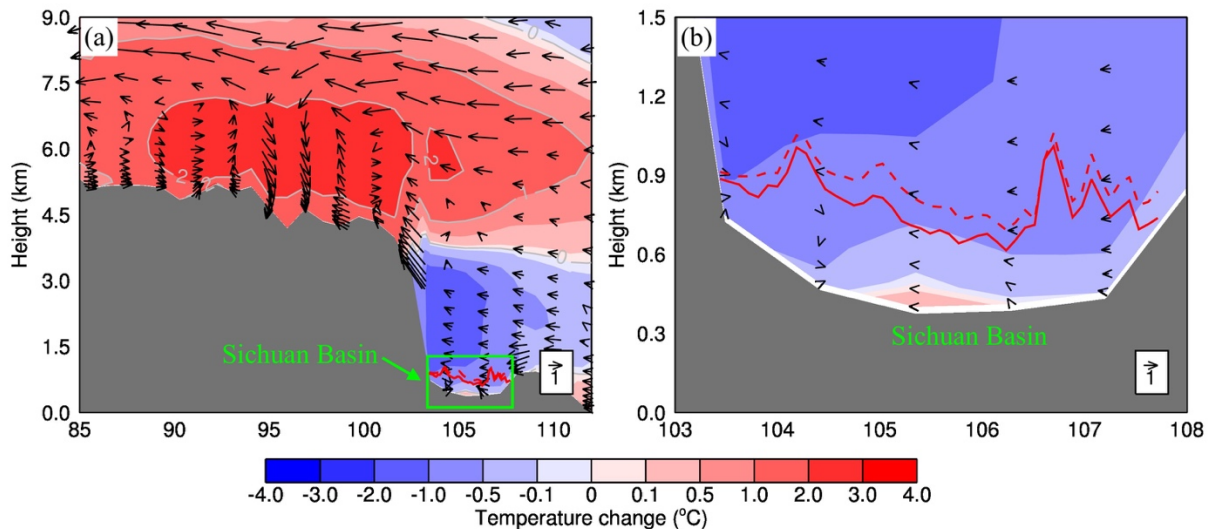


786

787 **Figure 9** Spatial change in the PBL height induced by 2°C warming over the Tibetan Plateau.
788 The positive shows the PBL height increases while the negative shows the PBL height
789 decreases.

790

791



792

793

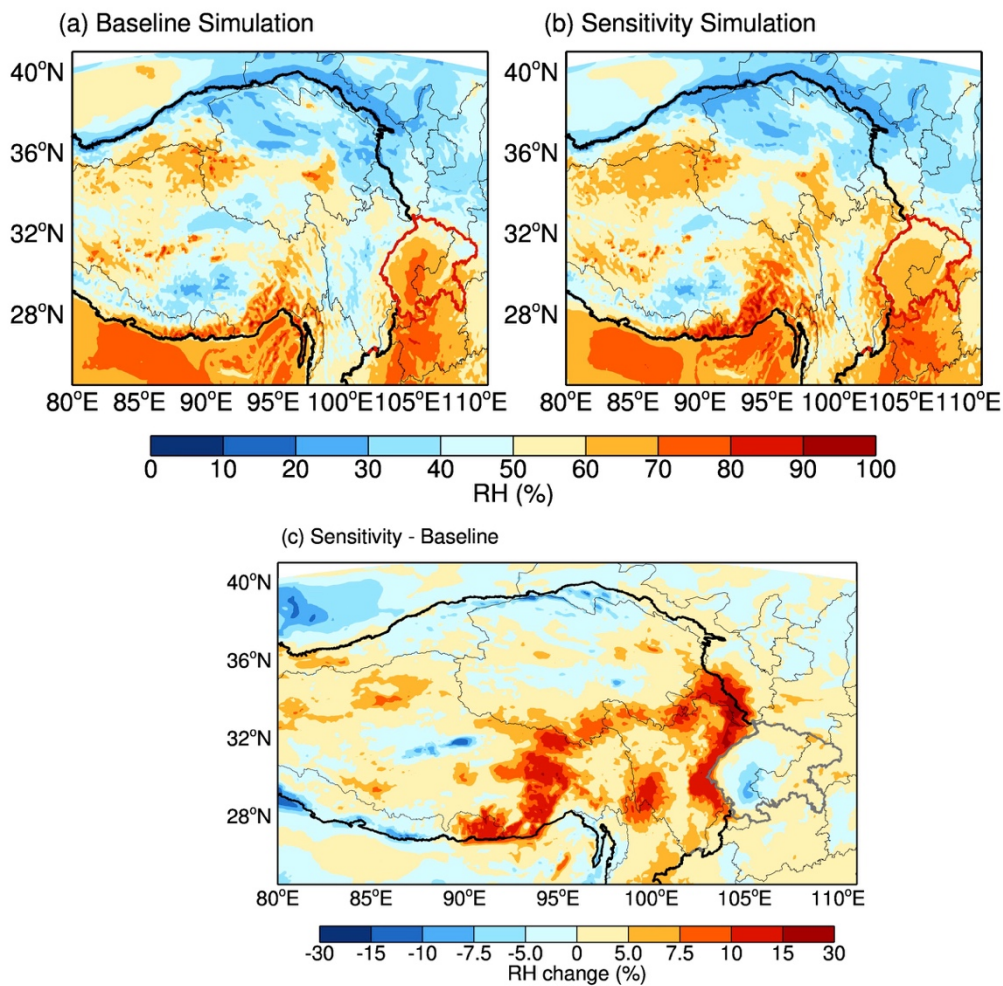
794

795

796

797

Figure 10 Vertical profiles of changes in temperature (shading and gray contour) and winds (arrows) along 30°N in January 2014. The gray shaded area presents topography. The green box for the Sichuan Basin, and the red solid (baseline simulation) and dash (sensitivity simulation) lines for the PBL height. (a) The Tibetan Plateau and Sichuan Basin, and (b) The Sichuan Basin.



799

800 **Figure 11** Comparison of spatial distributions of RH between (a) baseline simulation
 801 and (b) sensitivity simulation over the Tibetan Plateau and Sichuan Basin. (c) Similar
 802 to Figure 9, but for RH spatial changes when the plateau becomes 2°C warming, and
 803 the positive shows the RH increases while the negative shows the RH decreases.

804

805